Research Article | Vol. 27, No. 20 / 30 September 2019 / Optics Express 27761
Optics EXPRESS

Single is better than double: theoretical and experimental comparison between two thermal poling configurations of optical fibers

FRANCESCO DE LUCIA,[1] REX BANNERMAN,[1] NICOLAS ENGLEBERT,[2] MARTIN MIGUEL ANGEL NUNEZ VELAZQUEZ,[1] FRANCOIS LEO,[2] JAMES GATES,[1] SIMON-PIERRE GORZA,[2] JAYANTA SAHU,[1] AND PIER JOHN ANTHONY SAZIO[1,*]

[1] *Optoelectronics Research Centre, University of Southampton, SO17 1BJ, UK*
[2] *OPERA-Photonics, Université libre de Bruxelles, 50 av. F.D. Roosevelt, CP194/5, B-1050 Bruxelles, Belgium*
[*] *pjas@soton.ac.uk*

Abstract: Thermal poling, a technique to create permanently effective second-order susceptibility in silica optical fibers, has a suite of applications including frequency conversion and mixing for high harmonic generation and phase sensitive amplification, optical switching and modulation, and polarization-entangled photon pair generation. In this work, we compare both theoretically and experimentally two different electrode configurations for poling optical fibers, namely double-anode and single-anode, for two different geometries of the cladding holes. This analysis reveals that the single-anode configuration is optimal, both for the absolute value of effective $\chi^{(2)}$ created in the fiber core, and for the simplification of the fiber fabrication process.

1. Introduction

The thermal poling technique, invented at the beginning of the 90's by Myers *et al.* [1], is a method for creating a quadratic nonlinear optical response in centrosymmetric materials, which, in the dipole approximation, do not normally possess any $\chi^{(2)}$ [2]. Initially used for bulk glasses, the technique was later adopted to pole optical fibers, provided they were equipped with electrodes embedded inside cladding channels located adjacent to the fiber core [3]. Nevertheless, the early attempts of poling optical fibers in the conventional configuration anode-cathode (A-C), such as the ones reported in [3] and [4], were significantly limited by the short distance between the two electrodes (≈10 to 20 µm) which often produced electrical breakdown due to the high differences of potential applied, despite the relatively high dielectric strength of silica (a typical value of dielectric strength is the one reported in [5], of $8 \times 10^8 V/m$ for 6 µm thick silica samples).

In 2009 an important step further towards a better exploitation of the thermal poling technique was presented by the work of Margulis *et al.* [6], who introduced a new configuration for poling optical fibers, called thermal "charging". This technique is based on the observation that a depletion region and consequently effective second order susceptibility could be created via a thermal poling process where the two electrodes embedded in the two cladding channels of the fiber are both connected to the same positive electric potential. This new cathode-less configuration, also defined double-anode (D-A), allows for significantly reduced risk of breakdown between the two embedded electrodes and furthermore generates a $\chi^{(2)}$ higher than the one created via the conventional A-C configuration into the fiber core [6]. The geometry of the fiber used in the work of Margulis *et al.* is characterized by two cladding holes located at two different distances from the core, which is also the geometric center of the fiber (we will refer to this

#372200 https://doi.org/10.1364/OE.27.027761
Journal © 2019 Received 9 Jul 2019; revised 7 Aug 2019; accepted 7 Aug 2019; published 18 Sep 2019

Optics EXPRESS

configuration of electrodes as "asymmetric" from now on). The numerical model of the depletion region evolution in twin-hole asymmetric silica fiber poled in cathode-less configuration has been published in 2014 [7] by Camara *et al*.

In our work we apply the modified Camara model, developed by De Lucia *et al.* [8], to a fiber identical in terms of chemical composition and cladding/core sizes to the one considered in [6,7], but whose geometry is characterized by the fact that the two cladding holes are located at the same distance from the fiber core. This geometry of the fiber will be defined "symmetric" in the rest of the paper. The most relevant observation coming from our numerical study is that for long poling periods ($\approx$ 120 minutes) the value of $\chi^{(2)}_{eff}$ calculated from the distribution of the electric field frozen inside the symmetric fiber poled in D-A configuration is zero at the center of the fiber. This fact pushed us to investigate a different poling configuration, namely single-anode (S-A), where only one of the cladding holes of the fiber is equipped with an embedded electrode contacted to high positive voltages. The simulations indicate that in the same experimental conditions considered for the D-A poling, the S-A configuration shows a non-vanishing value of $\chi^{(2)}_{eff}$ at the center of the fiber's core.

Starting from this important theoretical result we first analyze the dynamics of the thermal poling process for both the poling configurations D-A and S-A and calculate the values of $\chi^{(2)}_{eff}$ at different positions along the line bisecting the two cladding holes. We then compare the two poling configurations in terms of the calculated nonlinear coefficient of the second harmonic generation κ, concluding that the S-A configuration is the most favorable. Furthermore, we find an experimental confirmation of this theoretical prediction. We indeed create two identical samples of asymmetric fiber and pole them in the same experimental conditions but in the two different poling configurations. In order to measure the values of κ the second order nonlinearity created in the two fibers has been periodically erased via UV exposure [9] to obtain the quasi-phase matching conditions around the wavelength of 1550 nm. The experimental comparison confirms that the best poling configuration is the S-A one in terms of κ for long poling periods (two hours). The S-A configuration also allows for a significant simplification of the fiber drawing process, as it does not require two precisely positioned holes inside the cladding preform as demanded by the D-A configuration.

2. 2D-numerical model of S-A configuration for thermal poling

The numerical simulations presented in this work are developed from the 2D-model originally implemented in [7] and subsequently modified in 2016 [8]. Both works are based on the model developed by Kudlinski *et al.* in [10], where two different types of charges are assumed to migrate under the effect of an externally applied electric field. In particular sodium (Na^+) is the cation of highest mobility in silica, and its displacement results in a cation depleted region of high electrical resistivity near the anodes embedded within a fused silica twin-hole fiber waveguide. The negatively charged, non-bridging oxygen sites left behind (uncompensated negative charges) can be considered motionless up to 300 °C. It is this charge separation that gives rise to the recorded field. The ions reaching the electrode-cladding surface or the air-cladding surface are assumed to recombine on these surfaces, rather than accumulate. If the poling process continues long enough ($\approx$ 2 hours), the width of the depletion region increases, but at the same time a second type of cation (with 10^3 times lower mobility [7]) is also driven into the glass (i.e. H_3O^+), which begins to neutralize the uncompensated negative charges. When both migration and diffusion are taken into account, the local equation of continuity and Poisson's equation lead to the following partial differential equation solved in x, y, and t:

$$\frac{\partial c_i}{\partial t} + \nabla \cdot (-D_i \nabla c_i - z_i \mu_i F c_i \nabla V) = R_i \tag{1}$$

Optics EXPRESS

where the index i represents one of the positive ionic species ($i = 1$ for sodium ions and $i = 2$ for the injected hydrogenated species), the first term in brackets accounts for diffusion and the second term corresponds to drift in the electric field. In Eq. (1), c is the concentration, D the diffusivity, z the charge, μ the ion mobility, F is Faraday's constant, V the electric potential and R the consumption or production rate, as detailed in [8]. The initial concentration of the Na^+ charges (uniformly distributed inside the cross section of the fiber) is 1 ppm, while the concentration of the H_3O^+ is initially null and then varies in time proportionally to the electric field at the interface hole/cladding, as suggested by Eq. (5) of [10]. The proportionality coefficient σ_2 is assumed identical to the one used in [10], that is $5 \cdot 10^{12} m^{-2} V^{-1} s^{-1}$. The chosen value for the mobility (at the temperature of 265 °C) of the Na^+ charges is $2 \cdot 10^{-15} m^2 V^{-1} s^{-1}$ while the mobility of the H_3O^+ is $2 \cdot 10^{-18} m^2 V^{-1} s^{-1}$, both in accordance with the values reported in [7]. The electric field and potential distribution as a function of poling duration are derived from Maxwell's equations in the electrostatic regime, from which it is possible to deduce the spatial distribution of the second-order nonlinearity within the fiber.

We first consider a fiber of 125 µm OD cladding with a Germania-doped glass core of 4 µm diameter and a 0.17 numerical aperture (NA). Two 27 µm diameter channels run adjacent to the fiber core at a distance of 10.4 µm (as measured from the closest edge of the empty channel with respect to the center of the core). The distance of each channel from the fiber core has been chosen to keep the overall distance between the two channels identical to the one considered in [6,7]. The two channels host the embedded electrodes which are both connected to a potential of + 6 kV. In the numerical model, realized in COMSOL^{TM} Multiphysics, the fiber is assumed to be located on top of a borosilicate microscope slide and the whole system is immersed in air and in the middle of a virtual metallic box whose walls (10 cm side length) are always held at ground potential.

The duration of the poling process has been chosen to be 7200 seconds in total. In order to make the numerical model more realistic, we assumed that after 7000 s the mobility of the impurities goes to zero (to simulate the cooling process of the glass) while 100 seconds later the anodic potential drops to zero (to simulate the removal of the externally applied electric field). Figure 1 shows the final concentration distribution of the fast (Na^+) and slow (H_3O^+) ions for the D-A poling configuration of the symmetric fiber.

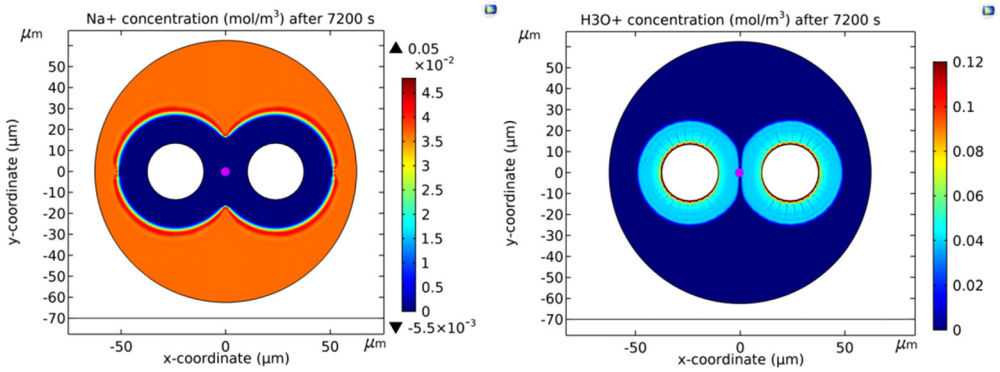

Fig. 1. Computed concentration distributions of the Na^+ impurity ions and hydrogenated species after 7200 s of thermal poling for a twin-hole fused silica fiber of symmetric geometry heated up at 265°C and poled in D-A configuration with an applied electric potential of 6 kV. The purple circle indicates the position of the core.

Figure 2 shows the temporal evolution of the electric potential in the fiber poled in D-A configuration while Fig. 3 reports the temporal evolution of the $\chi^{(2)}_{eff}$ value calculated at five

Optics EXPRESS

different positions in the XY-plane ((-2,0)μm, (-1,0)μm, (0,0)μm, (1,0)μm, (2,0)μm) and the curve representing the spatial trend of the $\chi^{(2)}_{eff}$ calculated after 7200 s of poling along the X axis (the axis along which the frozen-in electric field is assumed to be directed) in the spatial range between the two cladding holes. The values of $\chi^{(2)}_{eff}$ have been calculated using the formula [10]:

$$\chi^{(2)}_{eff} = 3\chi^{(3)}E_{dc} \tag{2}$$

where E_{dc} is the electric field frozen into the fiber after the thermal poling process ends and $\chi^{(3)}$ is the third order nonlinear susceptibility of the glass that the fiber is made from, which in the case of silica is assumed to be of $2 \times 10^{-22} m^2 V^{-2}$[11].

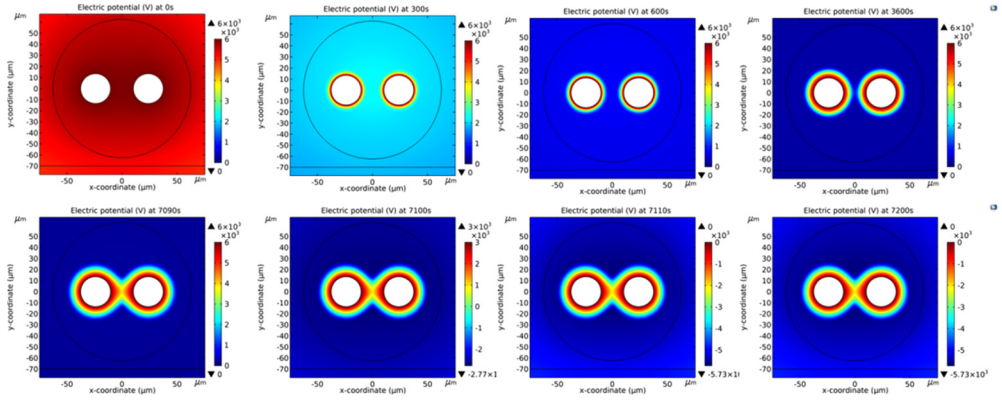

Fig. 2. Computed electric potential evolution during the thermal poling process for a twin-hole fused silica fiber of symmetric geometry poled in D-A configuration. The mobility of the Na^+ is assumed to go to zero at 7000 s while the electric potential externally applied is removed at 7100s. The fiber is located on top of a microscope slide made of borosilicate glass (1 cm of thickness, 7.5 cm of length and 2 cm of width), located at the center of a box of 10 cm of side length containing air. The ground of the system is assumed at the walls of the box.

In Fig. 3(b) is clear that in D-A poling configuration of a symmetric fiber $\chi^{(2)}_{eff}$ is basically zero at the core center. This behavior can be understood because of the mutually competitive action of the two electrodes. In order to circumvent this important drawback of the D-A configuration we decided to model a thermal poling experiment of the same symmetric fiber but in S-A configuration. This is characterized by a single electrode embedded inside one of the two cladding channels, while the other one is kept empty. All the other parameters of the poling experiment are otherwise identical to the D-A configuration.

The results of the numerical simulations are reported in Figs. 4, 5 and 6. In particular, for the S-A configuration reported in Fig. 6(b), the value of $\chi^{(2)}_{eff}$ calculated at the center of the core is completely different to the DA configuration. From this point of view it is expected that the S-A configuration allows for the creation of quadratic nonlinearity in a more efficient way than the D-A configuration.

Having confirmed the superior characteristics of the S-A poling configuration with respect to the D-A one, the same simulations were then realized for an asymmetric fiber [6,7]. The aim of these simulations is to confirm the results obtained so far and to compare them with the experimental results reported in section 4. In the asymmetric fiber, the two channels are located at a different distance with respect to the core's center, namely the nearest channel at 7.2 μm and the furthest channel at 13.6 μm (as measured from the closest edge of each channel). The

Optics EXPRESS

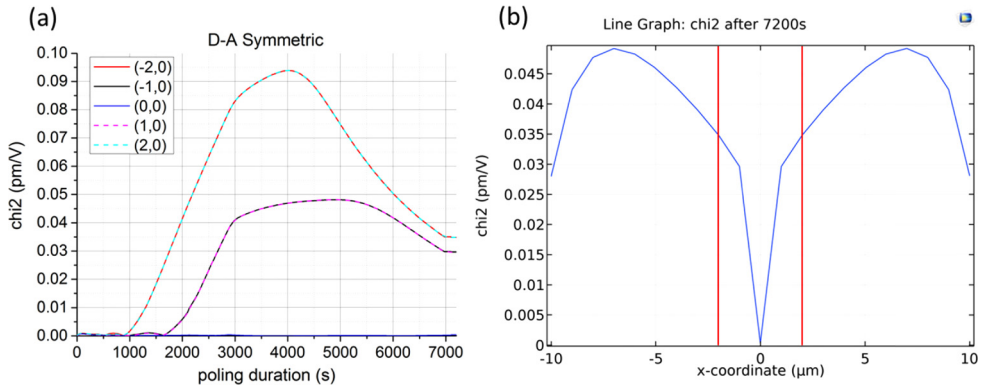

Fig. 3. (a) temporal evolution of the effective second order susceptibility calculated for a twin-hole fiber characterized by a symmetric geometry poled in D-A configuration. The anodic potential applied to each electrode is 6 kV. The values of $\chi^{(2)}_{eff}$ have been calculated with the formula reported in Eq. 2 at five different positions in the range covering the fiber's core diameter (4 µm) and in the plane Y = 0. In the Legend are reported the (x,y) coordinates expressed in µm of the points where the values of $\chi^{(2)}_{eff}$ have been calculated. (b) Line graph of the values of $\chi^{(2)}_{eff}$ calculated for a symmetric fiber poled in D-A configuration after 7200 s of poling, along the line bisecting the two cladding holes and crossing the fiber's center. The zero in the X-axis indicates the position of the fiber's center. The vertical red lines help to identify the core region.

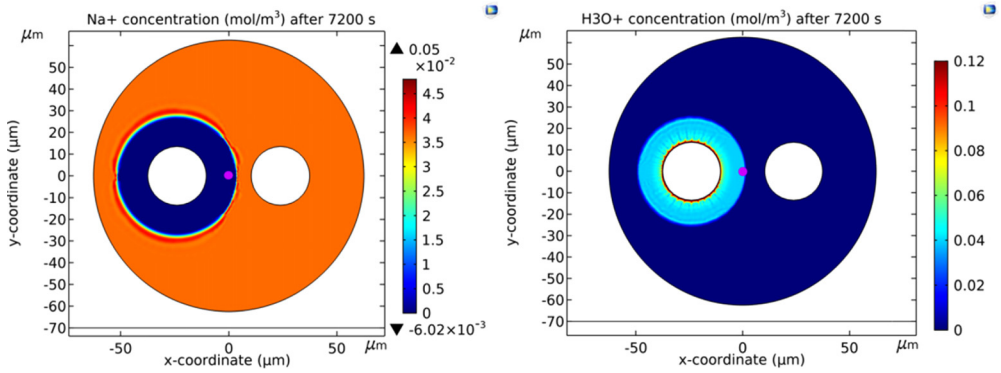

Fig. 4. Computed concentration distributions of the Na^+ impurity ions and hydrogenated species after 7200 s of thermal poling for a twin-hole fused silica fiber of symmetric geometry heated up at 265°C and poled in S-A configuration with an applied electric potential of 6 kV. The purple circle indicates the position of the core.

two poling configurations (D-A and S-A) have been modelled under the same conditions as the symmetric fiber. The results of these simulations are reported in Figs. 7, 8 and 9.

Due to the asymmetric nature of the fiber, it is clear from Fig. 9(a) that, in case of D-A configuration, the $\chi^{(2)}_{eff}$ value calculated after 7200 s of thermal poling is no longer zero at the center of the core. Nevertheless, even in this scenario the S-A poling configuration is still more effective than the D-A one. We can state that the absolute value of $\chi^{(2)}_{eff}$ obtained in S-A configuration inside the core region for long poling durations is larger than that obtained in D-A configuration. This result is expected in the S-A configuration due to the lack of competitive action of two positive electric potentials that is typical of the D-A configuration.

Optics EXPRESS

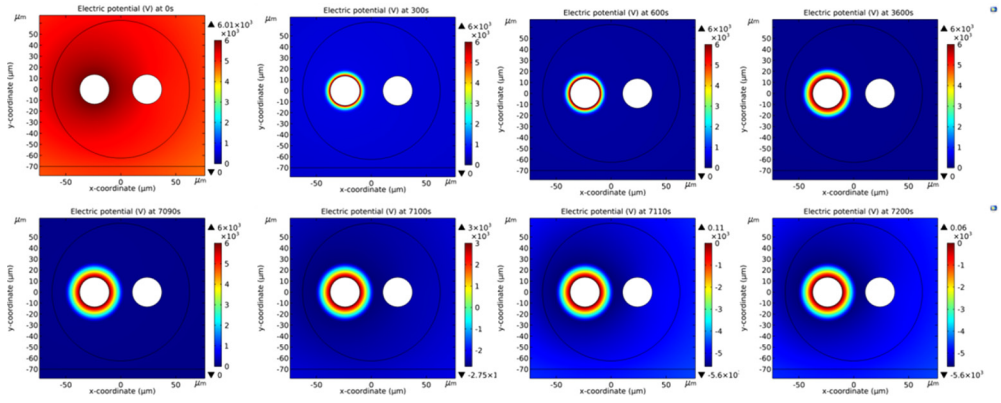

Fig. 5. Computed electric potential evolution during the thermal poling process for a twin-hole fused silica fiber of symmetric geometry poled in S-A configuration. The mobility of the Na^+ is assumed to go to zero at 7000 s while the electric potential externally applied is removed at 7100s. The fiber is located on top of a microscope slide made of borosilicate glass (1 cm of thickness, 7.5 cm of length and 2 cm of width), located at the center of a box of 10 cm of side length containing air. The ground of the system is assumed at the walls of the box.

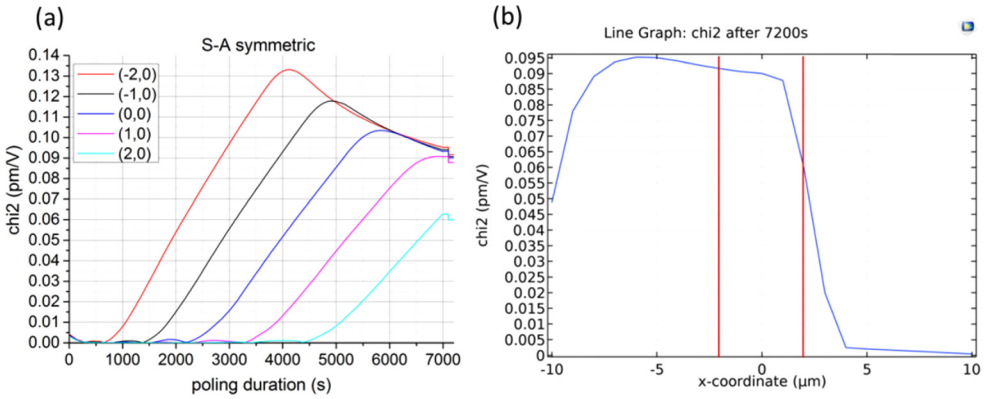

Fig. 6. (a) temporal evolution of the effective second order susceptibility calculated for a twin-hole fiber characterized by a symmetric geometry of the cladding channels (10.4 μm of distance between each cladding channel edge closest to the core and the center of the fiber) and poled in S-A configuration. The anodic potential applied to the embedded electrode is 6 kV. The values of $\chi^{(2)}_{eff}$ have been calculated with the formula reported in Eq. 2 at five different positions in the range covering the core diameter (4 μm) and in the plane Y = 0. The legend shows the (x,y) coordinates expressed in μm of the points where the values of $\chi^{(2)}_{eff}$ have been calculated. (b) Line graph of the values of $\chi^{(2)}_{eff}$ calculated for a symmetric fiber poled in S-A configuration after 7200 s along the line bisecting the two cladding holes and bisecting the center of the fiber. The zero in the X-axis indicates the position of the fiber's center. The vertical red lines help to identify the core region.

Optics EXPRESS

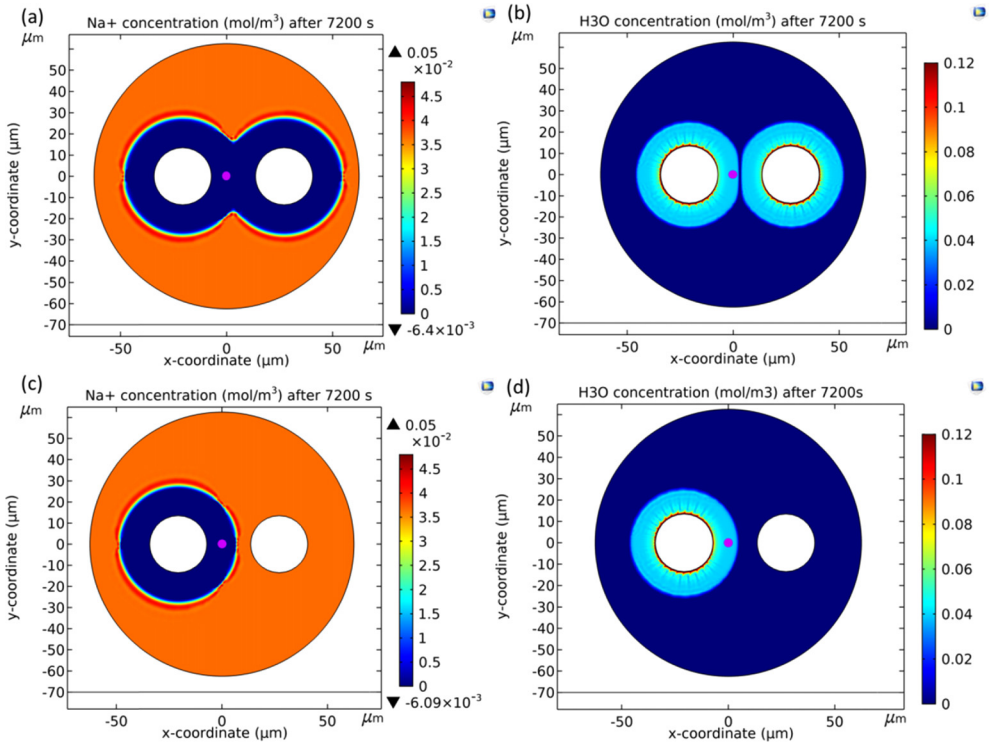

Fig. 7. Computed concentration distributions of the Na^+ impurity ions and hydrogenated species after 7200 s of thermal poling of a twin-hole fused silica fiber characterized by an asymmetric geometry. Two different electrode configurations are shown, namely double-anode (a) and (b) and single-anode (c) and (d). The temperature of poling is 265 °C. The geometry is identical to the fiber reported in [6,7]. The anodic potential of each configuration is + 6 kV. The purple circle indicates the position of the core.

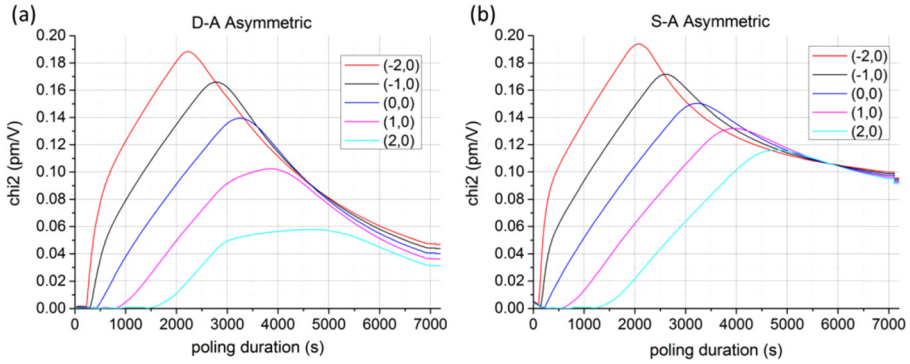

Fig. 8. Temporal evolution of the effective second order susceptibility calculated for a twin-hole fiber characterized by an asymmetric geometry of the cladding channels and poled in two different electrodes configurations, namely D-A (a) and S-A (b). The values of $\chi^{(2)}_{eff}$ have been calculated with the formula reported in Eq. 2 at five different positions in the range covering the core diameter (4 µm) and in the plane Y = 0. The legend shows the (x,y) coordinates expressed in µm of the points where the values of $\chi^{(2)}_{eff}$ have been calculated.

Optics EXPRESS

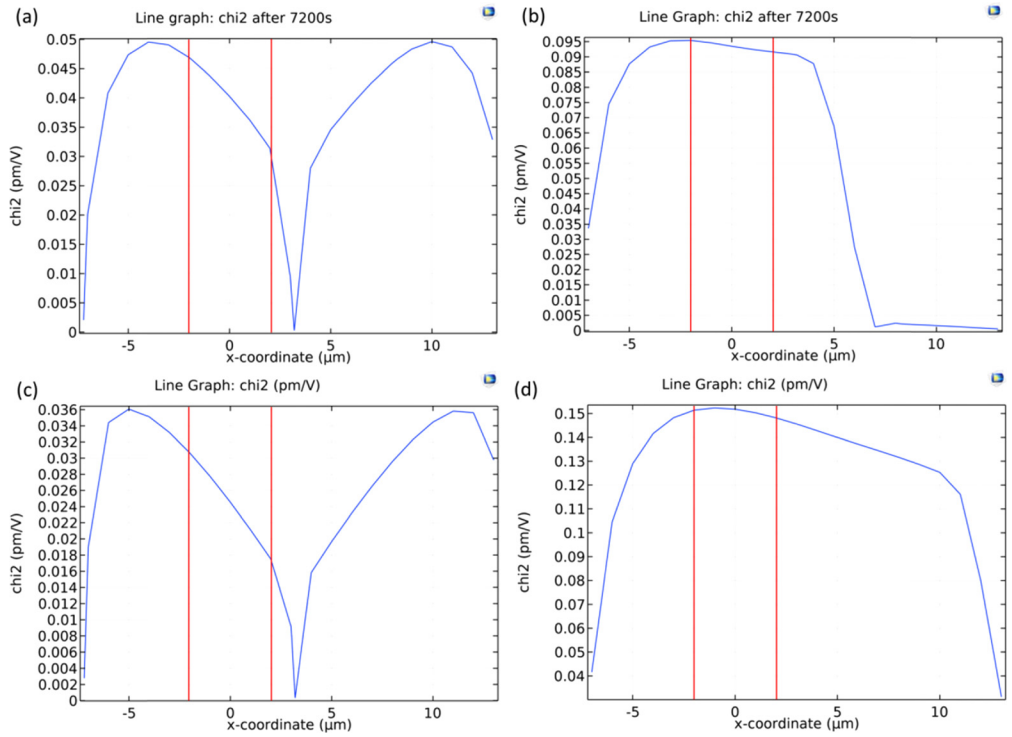

Fig. 9. Line graphs of the values of $\chi^{(2)}_{eff}$ calculated for an asymmetric fiber poled at 6 kV in D-A (a) and S-A (b) configuration after 7200 s, along the line bisecting the two cladding holes and bisecting the center of the fiber. (c) and (d) show line graphs of the values of $\chi^{(2)}_{eff}$ calculated for an asymmetric fiber poled at 15 kV respectively in D-A and S-A configuration after 7200 s, along the line bisecting the two cladding holes and bisecting the center of the fiber. The zero in the X-axis indicates the position of the fiber's center. The vertical red lines help to identify the core region.

This result allows for a significant simplification of fiber fabrication process and associated manufacturing tolerances as it only requires a single hole instead of two whilst simultaneously removing all the issues related to the precise location of the two cladding channels with respect to the core to optimize the value of $\chi^{(2)}_{eff}$. Our modeling confirms that the single-anode configuration can tolerate far higher positioning error due to the very stable dependence of the quadratic nonlinearity with respect to the relative position of the core and electrode.

It is interesting to note that as absolute value of the applied voltage increases, the competitive action of the two electrodes in D-A configuration becomes more and more significant. In contrast, higher values of electric potential applied to the S-A single embedded electrode will result in higher values of $\chi^{(2)}_{eff}$ in an even larger area surrounding the fiber core. Figures 9(c) and 9(d) show the line graphs of $\chi^{(2)}_{eff}$ numerically calculated for two (D-A and S-A) thermal poling processes with a positive potential of 15 kV applied.

3. Enhancement of the nonlinear effective coefficient by the poling configuration

The comparison between the two poling configurations (namely S-A and D-A) both experimentally and theoretically can be considered by the nonlinear coefficient of the propagation SHG process,

Optics EXPRESS

κ. If we write the two equations describing the spatial evolution along the propagation axis z of the amplitudes of the electric fields $E_1(\omega_1)$ and $E_2(2\omega_1)$ as [12]:

$$\frac{\partial A_1(z,t)}{\partial z} = i\kappa A_1^*(z,t)A_2(z,t)e^{-i\Delta\beta z} \tag{3}$$

$$\frac{\partial A_2(z,t)}{\partial z} = i\kappa A_1^2(z,t)e^{i\Delta\beta z} \tag{4}$$

where A_1 and A_2 are the slowly varying envelopes of the pump and the SH expressed in $\sqrt{W}$, $\Delta\beta = 2\beta_1 - \beta_2$ and the effective nonlinear coefficient κ is defined as:

$$\kappa = \frac{3\omega_1^2\chi^{(3)}}{\beta_1 c^2}\sqrt{\frac{2}{cn_{eff}^{2\omega}\varepsilon_0}}\frac{\iint (F_1^*(x,y))^2 F_2(x,y)E_{dc}(x,y)dxdy}{\iint |F_1(x,y)|^2 dxdy} \tag{5}$$

where $F_i(i = 1, 2)$ is the spatial profile of the modes normalized such as:

$$\iint |F_i(x,y)|^2 dxdy = 1 \tag{6}$$

The expression of κ in Eq. (5) takes into account the fact that the electric field E_{dc} created via thermal poling and numerically calculated shows a spatial distribution over the cross section of the fiber and that the effective nonlinearity has to be weighed by modal overlap between the fundamental and the SH wave.

The theoretical values of κ can be obtained from the Eq. (5) where the normalized spatial profiles of the two modes F_1 and F_2 and the value of $n_{eff}^{2\omega}$ have been obtained numerically via COMSOL^{TM} Multiphysics for a fiber of asymmetric geometry, and the $E_{dc}(x,y)$ values have been numerically calculated for the two different configurations of poling. The step-index fiber considered has a 4 µm diameter and an *NA* of 0.17. In Fig. 10 are reported the profiles of the norm of the electric fields of the fundamental modes of the pump and second harmonic waves guided inside a fiber characterized by an asymmetric geometry.

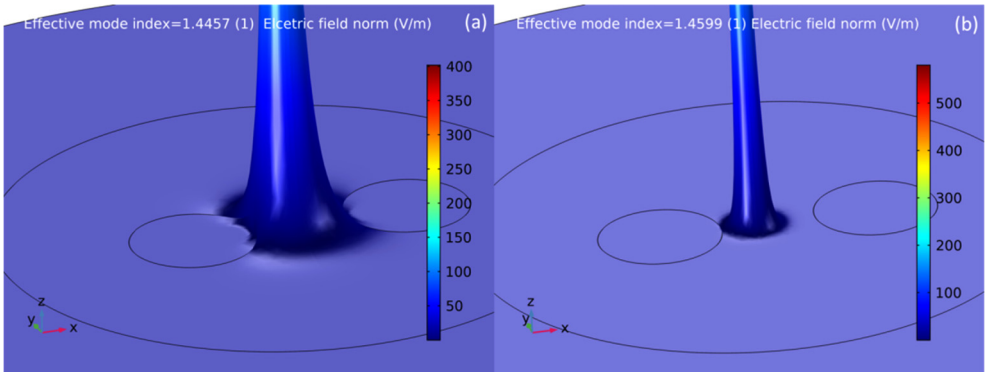

Fig. 10. Electric field norm profiles, numerically simulated in COMSOL^{TM} Multiphysics, of the fundamental modes of (a) pump (1550 nm) and (b) second harmonic (775 nm) waves guided in a fiber characterized by an asymmetric geometry. In both the pictures the hole on the left is the one closer to the fiber's core.

The area of investigation for the numerical simulations is the squared space limited by the points of coordinates x and y (-7, 7), (13, 7), (-7, -7) and (13, -7)µm. The ratio of the effective

Optics EXPRESS

nonlinear coefficients obtained in the two different poling configurations is:

$$\left(\frac{\kappa_{S-A}}{\kappa_{D-A}}\right)_{num} = 2.31 \tag{7}$$

This value can be compared to the experimental case.

4. Experimental determination of κ for the two poling configurations of PPSF

The numerical result of Eq. (7) indicates that the S-A configuration is superior to D-A due to the higher absolute values of κ obtained under the same poling conditions. In order to prove the validity of our theoretical predictions, in this section we provide experimental evidence. A sample identical to the one considered in Fig. 7 has been fabricated starting from a preform made of HSQ300 glass with a Germania doped core. The fiber has been fabricated in-house at the ORC, Southampton.

4.1. Fabrication of the PPSFs

The fiber used in the experiments of this work has been fabricated starting from tubes of Heraeus HSQ300 silica glass. Initially a process of MCVD has been adopted to deposit Germania inside the tube, which is then stretched to create the central part of the preform. The final preform was created via subsequent processes of over-sleeving, until the desired ratio core/cladding has been obtained. Finally the two holes were drilled inside the preform and the fiber drawn. The fiber created possesses a step-index profile.

Two 100 cm long fibers taken from the same reel of fused silica twin-hole (asymmetric) fiber were thermally poled under the same experimental conditions and in two different electrode configurations. The setup adopted for realizing the poling process is shown in Fig. 11. It consists of a heater of 60 cm total length, on top of which a borosilicate glass slab is fixed. The external metallic surface of the heater is connected to the ground of the High Voltage (HV) power supply and the role of the glass slab is to reduce the risk of breakdown between the electrodes embedded into the fibers to be poled and the ground.

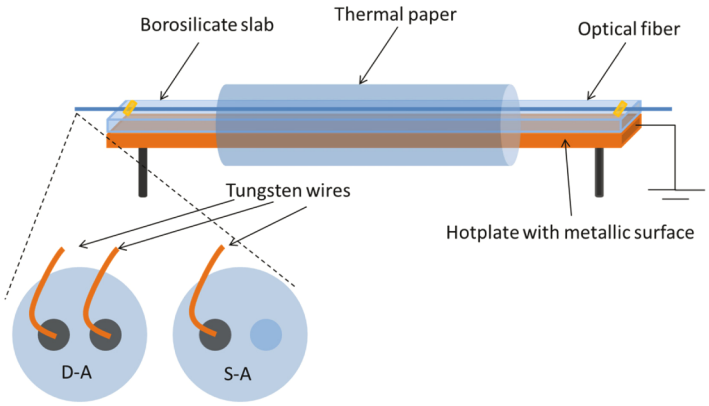

Fig. 11. Experimental setup used to pole the twin-hole silica fibers, either in D-A or in S-A configuration. The dark circles in the cross sections of the fiber represent the cladding channels filled with Mercury, while the pale blue one is empty. The use of epoxy resin to block one of the two channels allows for filling selectively only one of the two channels. A tungsten wire is immersed inside the Mercury for few mm in order to guarantee the electrical contact between the externally applied electric potential and the liquid embedded electrode and a drop of superglue is used to seal properly each end of the fiber.

Optics EXPRESS

The temperature of poling has been chosen to be 250 °C, while the anodic potential applied to each of the electrodes, in both the configurations, is 6 kV (provided by the HV supply). The chosen duration of each thermal poling process is 120 minutes. Two samples have been poled in these experimental conditions with both electrode configurations (S-A and D-A). The cladding channels of the fiber to be poled are filled with mercury using a pressurization system similar to the one adopted by Fokine *et al.* in [13]. Then a tungsten wire is inserted at one of the two ends of the fiber and in each of the channels previously filled with mercury such that it is possible to contact the liquid electrode with the HV supply. A tiny amount of glue is then used to seal each end of the fiber. After the poling process ends, the metal is removed using the same pressurization system and the fiber can be periodically erased for QPM, as described in the next sections.

It is well known that in non-centrosymmetric media it is possible to observe quadratic nonlinear phenomena such as for example SHG, optical rectification, as well as sum and difference frequency generation (SFG and DFG respectively). However, in order to observe these effects, it will be necessary to create the conditions of phase matching (PM), which consists in the coincidence of the phase velocity of the two waves involved in the second order nonlinear effect desired. But in a dispersive medium the PM condition for the wavelengths involved in the nonlinear process in the same propagation mode is not possible to fulfil.

In 1962 Armstrong *et al.* [14] proposed the quasi-phase matching (QPM) method to overcome the drawback of wave-vector mismatch in dispersive media, in which it is compensated by modulating the quadratic nonlinearity. If the nonlinear coefficient is a periodic function of period Λ, along the light propagation direction, the wave-vector mismatch between the pump and second harmonic becomes ΔK_q, where q is an integer that defines the order of QPM. To first order, the condition of QPM is given by the following equation:

$$\Delta K = \frac{4\pi}{\lambda} n_{eff}^{2\omega} - 2\frac{2\pi}{\lambda} n_{eff}^{\omega} - \frac{2\pi}{\Lambda_{QPM}} = 0 \tag{8}$$

where n_{eff} is the effective refractive index of the propagating modes. From the Eq. (8) we can obtain the expression of the QPM period required at the λ_{QPM}, which is given by the following:

$$\Lambda_{QPM} = \frac{\lambda_{QPM}}{2(n_{eff}^{2\omega} - n_{eff}^{\omega})} \tag{9}$$

In order to measure the efficiency of SHG and consequently the nonlinear coefficeint κ it is necessary to erase periodically the poled samples with the correct period allowing for QPM at the desired wavelength. The nonlinearity is erased by illuminating the core region of the poled fiber with UV light. A generally accepted explanation of the phenomenon of UV erasure is that exposure to high energy photons leads to the release of electrons, which move through the electric field frozen into the fiber by thermal poling and annihilate it [15].

From the Eq. (9) it should be possible to calculate precisely the period of grating necessary to obtain QPM at a desired wavelength, but this is difficult in practice due to the difficulty of calculating precisely the values of effective refractive indices at the two wavelengths. Consequently, in order to identify the correct period of erasure of the nonlinearity a preliminary experimental study needs to be performed which consists in erasing the nonlinearity created inside the poled fiber with different periods and looking for the wavelength doubled via SHG at each period. After few tests, it was identified that for the particular fiber used to fabricate PPSFs, a period of erasure of 55 µm is suitable to obtain frequency doubling at approximately 1550 nm. A grating of 10 cm of length with the same period was written on the two asymmetric samples, namely D-A and S-A. The setup for erasing the nonlinearity is sketched in Fig. 12.

The UV light source is CW argon ion laser frequency doubled to 244 nm, with an acousto-optic modulator (AOM, Gooch and Housego: M110-10UV-SU8) used to modulate the laser output. The laser is focused to a circular spot, 20 µm in diameter, above an Aerotech A3200 four axis

Optics EXPRESS

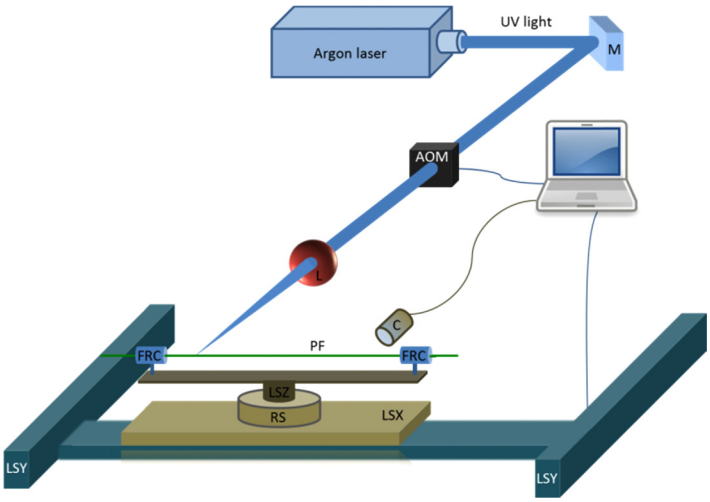

Fig. 12. Setup for UV erasure of poled fibers. The acousto-optic modulator (AOM) is synchronized with the motion of the linear stage (LSX) via a control system (PC) to shut the beam in order to obtain the desired duty cycle and period of erasure. M stands for mirror, L for lens, FRC for fiber rotator clamp, PF is the poled fiber, C is the camera, RS is a rotation stage, LSX, LSY and LSZ are three linear stages for the three different directions.

linear stage. The poled fiber to be UV erased is clamped onto the linear stage by two fiber rotator clamps, with one clamp mounted on a vertical axis manual translation stage and the other mounted on a force gauge. Using the force gauge the fiber is tensioned to 0.3 N. A microscope camera is then used to align the fiber core to the laser spot along the 30 cm of fibre the linear stage can translate across. The laser is modulated using the AOM while translating the fiber core through the spot to achieve a grating of the desired duty cycle and period. For the gratings presented here a fluence of 14 J/cm^2 and a duty cycle of 5% have been used to periodically erase the nonlinearity.

4.2. *Experimental measurement of κ in both poling configurations*

In order to verify the theoretical predictions of Eq. (7), we decided to experimentally determine the nonlinear coefficient κ for both the poling configurations. The integration of Eq. (4) in the approximation of un-depleted pump opens to way to this measurement. This approximation assumes that the energy transfer from the fundamental field A_1 to the second harmonic field A_2 is weak compared to the energy contained in field A_1. Under this assumption and with the initial condition $A_2(z = 0) = 0$, the integration over the distance L leads to the following expression:

$$A_2(z) = i\kappa|A_1|^2 e^{i\Delta\beta L} L\text{sinc}\left(\frac{\Delta\beta L}{2}\right) \tag{10}$$

The Eq. (10) takes a simple form when the phase matching condition is verified. With the definition of kappa, the square modulus of the field gives the intensity in watt. Experimentally, we can therefore obtain:

$$P_{out}^{2\omega} = \kappa^2 L^2 (P_{out}^{\omega})^2 \tag{11}$$

where $P_{out}^{2\omega} = |A_2|^2$ and $P_{out}^{\omega} = |A_1|^2$. Changing the power of the fundamental field, we can measure κ experimentally. The setup to perform this measurement is shown in Fig. 13.

Each characterized sample consists of the PPSF (approximately 20 cm in length) with both ends spliced to a piece of step index fiber (Thorlabs, SM980) approximately 30 cm in length.

Optics EXPRESS

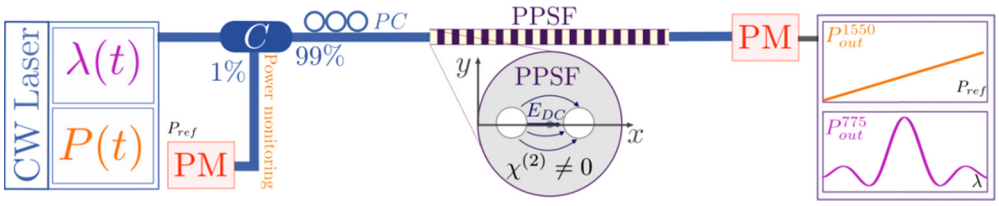

Fig. 13. Experimental setup for the PPSF's nonlinear characterization: CW Laser is a continuous wave narrowband tunable laser (Agilent, model 8164B, linewidth ≈ 100 kHz), P stands for the power and λ for the wavelength of the laser, C is the optical coupler, PC is the inline polarization controller, $PPSF$ is the periodically poled silica fiber, PM are power meters.

The splice process of the periodically poled twin-hole silica fiber (PPSF) with a solid cladding fiber has been optimized experimentally (with three different splicer manufacturer models) by modifying some of the parameters of the splice process, such as for example the gap between the two fibers, the voltage and the duration of the electric arc applied to fuse the facets of the two fibers and the position of the arc applied with respect to the two fibers facets. The splice itself represented a challenge because of the presence of the two holes in the cladding of the PPSF. If the voltage, the duration and the position of the arc are not optimized appropriately, the splice process can cause the collapse of the twin-hole fiber with a consequent failure of the splice. According to our experience, the average value of splice losses measured over a series of periodically poled samples is ~ 0.5 dB. Assuming that the presence of the holes makes the splice challenging, we believe that the presence of just one hole instead of two would simplify the process. At the moment this is a working assumption that we will be able to confirm experimentally in the next future.

Initially, a pump wavelength ramp centered at 1550 nm and 20 nm wide is performed in order to find λ_{QPM}. To do this, a silicon photodiode power sensor sensitive in the range 300 - 1100nm was used to measure only the optical power associated with the second harmonic light and not the pump.

When the input pump polarization state does not match one of the linear birefringent axes of the fiber, three peaks are seen in the SHG signal. The birefringence of the fiber is due to its geometry and to the different stresses induced during the fiber drawing process along the two different directions X and Y (X is the direction of the frozen-in electric field E_{dc}, Y is the direction orthogonal to X and located in the plane of the fiber's cross section, as shown in Fig. 13). The three peaks are due to the fact that, because of the birefringence of the sample, it is possible to spectrally separate three different SHG processes. If we assume that the principal polarization axes of the fiber are aligned along X and Y, the QPM condition in the PPSF is given by [16]:

$$\beta_i^{\omega_F} = \beta_j^{\omega_F} + \beta_k^{\omega_F} + \frac{2\pi}{\Lambda} \tag{12}$$

where ω_F corresponds to the frequency of the fundamental harmonic, β_s are the propagation constants, $i, j, k (= XorY)$ indicate the polarization of the waves, and Λ is the first order QPM period of the nonlinearity erasure. We define QPM of type-I the case where $j = k$, and type-II the case where $j \neq k$. So, in a random state of the incoming light polarization the first two peaks correspond to a SHG process of type-I (respectively $Y + Y \rightarrow X$ and $X + X \rightarrow X$) while the third peak visible corresponds to the type-II process ($X + Y \rightarrow Y$). As a point of interest, the inverse process (spontaneous parametric down conversion, SPDC) of this last type-II parametric up-conversion can be exploited to generate polarization-entangled photon pairs in a periodically poled fiber, as reported for example in [17]. The PPSF is now pumped at a wavelength corresponding to the second harmonic and will result in the production of type-II

Optics EXPRESS

down-converted photon pairs centered at the wavelength of the fundamental harmonic, also in the LP_{01} mode. If the incident photon possesses a polarization state along the Y axis, the two photons generated are characterized by orthogonal polarization states (respectively along X and Y), in other words are polarization entangled.

After seeing the three peaks, by using the polarization controller (PC) shown in Fig. 13, it is possible to align the polarization along the axis X, consequently maximizing the peak corresponding to the process $X + X \rightarrow X$, which is the one where the $\chi^{(2)}_{eff}$ assumes its maximum value. In Fig. 14 are reported the tuning curves of each sample obtained and normalized at the maximum value of SH signal for the two poling configurations. In these conditions, we measured respectively the power of the SH signal after the PPSF ($P^{2\omega}_{out}$), the power of the pump after the PPSF (P^{ω}_{out}) and the power of the incoming pump before the PPSF (P^{ω}_{in}). With these measurements, the ratio $\kappa_{S-A}/\kappa_{D-A}$ has been obtained:

$$\left(\frac{\kappa_{S-A}}{\kappa_{D-A}}\right)_{\text{exp}} \approx \frac{0.0565}{0.027} \cdot \frac{m^{-1}W^{-0.5}}{m^{-1}W^{-0.5}} \approx 2.09 \tag{13}$$

This experimental value confirms the theoretical predictions given by the expression reported in Eq. (7) in terms of the ratio between the nonlinear coefficients produced in the two different poling configurations. It is worth highlighting that for the same period of erasure of the nonlinearity, the QPM wavelength is slightly different for the two fibers (taken from the same sample and poled under the same experimental conditions, apart from the different S-A vs D-A configurations). In particular the asymmetric D-A sample shows QPM at 1.5647 μm, while the asymmetric S-A one at 1.5662 μm. However, the difference between the two QPM wavelengths of the two poled fibers of the same geometry is of the order of few nanometers, perfectly compatible with the tolerances of the grating fabrication process itself [18].

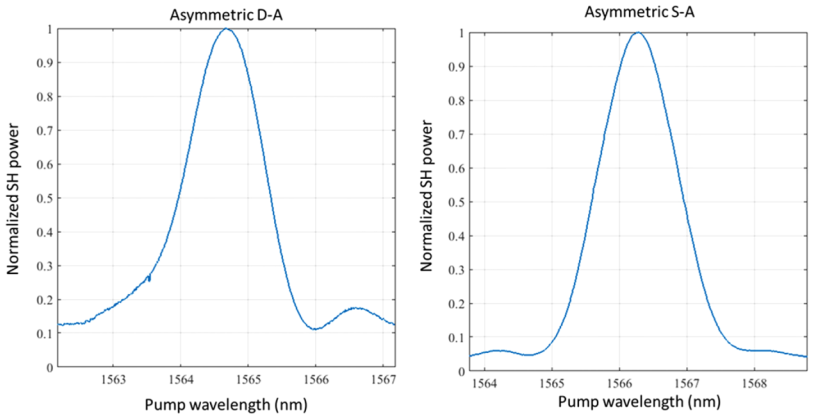

Fig. 14. Tuning curves obtained for the two different samples pumped with a narrowband CW laser in the conditions of pump polarization which maximize the SH signal for the SHG process of type-I ($X + X \rightarrow X$). The sensor used to measure the SH signal is a silicon photodiode power sensor (Thorlabs, model S150C).

5. Conclusions

In conclusion, we have presented 2D numerical simulations and experimental verification of thermally poled twin-hole, step index silica optical fibers in D-A and S-A configurations. Finite element analysis of the space-charge region formation reveals that the single-anode configuration represents the best possible choice. This is due to the absence of competitive space-charge

Optics EXPRESS

evolution with another electrode, as is the case in the double-anode configuration. This detrimental effect means that, for long time poling (2 hours), the superior S-A configuration not only allows for a value of $\chi^{(2)}_{eff}$ approximately double with respect to that attainable for D-A, but in addition, this value, for a range of positions around the fiber core, is almost independent of the relative position of the fiber core with respect to the electrodes. This is highly advantageous for relaxing the constraints of fiber fabrication as it is possible to tolerate far higher manufacturing error with respect to the relative position of the core and electrode. The results of the numerical simulations have been confirmed experimentally via the measurement of the SHG coefficients κ for S-A and D-A. This work represents not only a further step towards the full understanding of the dynamics of the thermal poling process but also an important contribution for an optimal exploitation of this technique in the area of all-fiber quadratic nonlinear photonics.

Funding

Engineering and Physical Sciences Research Council (EP/I035307/1, EP/K034480/1, EP/M013243/1, EP/M024539/1); Fonds pour la Formation à la Recherche dans l'Industrie et dans l'Agriculture; H2020 European Research Council (757800).

Acknowledgments

The authors acknowledge Andrea Ventura, Peter Shardlow and Vassili Savinov for interesting discussions and tips about the study of light guidance in optical fibers and mesh issues. The datasets of this work can be found at: https://doi.org/10.5258/SOTON/D0956.

References

1. R. A. Myers, N. Mukherjee, and S. R. J. Brueck, "Large second-order nonlinearity in poled fused silica," Opt. Lett. **16**(22), 1732–1734 (1991).
2. U. Osterberg and W. Margulis, "Dye laser pumped by Nd:YAG laser pulses frequency doubled in glass optical fiber," Opt. Lett. **11**(8), 516–518 (1986).
3. D. Wong, W. Xu, S. Fleming, M. Janos, and K.-M. Lo, "Frozen-in electrical field in thermally poled fibers," Opt. Fiber Technol. **5**(2), 235–241 (1999).
4. P. Blazkiewicz, W. Xu, D. Wong, and S. Fleming, "Mechanism for thermal poling in twin-hole silicate Fibers," J. Opt. Soc. Am. B **19**(4), 870–874 (2002).
5. F. Haberl, J. Hochreiter, J. Zehetner, and A. J. Smith, "Electrical breakdown in ge-doped silica glass fibers," International Journal of Optoelectronics **5**(4), 363–366 (1990).
6. W. Margulis, O. Tarasenko, and N. Myrén, "Who needs a cathode? Creating a second-order nonlinearity by charging glass fiber with two anodes," Opt. Express **17**(18), 15534–15540 (2009).
7. A. Camara, O. Tarasenko, and W. Margulis, "Study of thermally poled fibers with a two-dimensional model," Opt. Express **22**(15), 17700–17715 (2014).
8. F. De Lucia, D. Huang, C. Corbari, N. Healy, and P. J. A. Sazio, "Optical fiber poling by induction: analysis by 2D numerical modeling," Opt. Lett. **41**(8), 1700–1703 (2016).
9. A. Canagasabey, M. Ibsen, K. Gallo, A. V. Gladishev, E. M. Dianov, C. Corbari, and P. G. Kazansky, "Aperiodically poled silica fibers for bandwidth control of quasi-phased-matched second-harmonic generation," Opt. Lett. **35**(5), 724–726 (2010).
10. A. Kudlinski, Y. Quiquempois, and G. Martinelli, "Modeling of the $\chi^{(2)}$ susceptibility time-evolution in thermally poled fused silica," Opt. Express **13**(20), 8015–8024 (2005).
11. A. C. Liu, M. J. F. Digonnet, and G. S. Kino, "Measurement of the dc Kerr and electrostrictive phase modulation in silica," J. Opt. Soc. Am. B **18**(2), 187–194 (2001).
12. R. W. Boyd, "Nonlinear optics", 3rd ed. Academic Press, 2008.
13. M. Fokine, L. E. Nilsson, A. A. Claesson, D. Berlemont, L. Kjellberg, L. Krummenacher, and W. Margulis, "Integrated fiber Mach-Zehnder interferometer for electro-optic switching," Opt. Lett. **27**(18), 1643–1645 (2002).
14. J. A. Armstrong, N. Bloembergen, J. Ducuing, and P. S. Pershan, "Interactions between light waves in a nonlinear dielectric," Phys. Rev. **127**(6), 1918–1939 (1962).
15. F. Ouellette, K. O. Hill, and D. C. Johnson, "Light induced erasure of self-organized $\chi^{(2)}$ gratings in optical fibers," Opt. Lett. **13**(6), 515–517 (1988).
16. E. Y. Zhu, L. Qian, L. G. Helt, M. Liscidini, J. E. Sipe, C. Corbari, A. Canagasabey, M. Ibsen, and P. G. Kazansky, "Measurement of $\chi^{(2)}$ symmetry in a poled fiber," Opt. Lett. **35**(10), 1530–1532 (2010).

Optics EXPRESS

17. E. Y. Zhu, Z. Tang, L. Qian, L. G. Helt, M. Liscidini, J. E. Sipe, C. Corbari, A. Canagasabey, M. Ibsen, and P. G. Kazansky, "Direct generation of polarization-entangled photon pairs in a poled fiber," Phys. Rev. Lett. **108**(21), 213902 (2012).
18. M. M. Fejer, G. A. Magel, D. H. Jundt, and R. L. Byer, "Quasi-phase matched second-harmonic generation: tuning and tolerances," IEEE J. Quantum Electron. **28**(11), 2631–2654 (1992).